Strain-induced phase transition in -MnO_2

2012 EPL 99 27005

(http://iopscience.iop.org/0295-5075/99/2/27005)

A Letters Journal Exploring the Frontiers of Physics

July 2012

EPL, **99** (2012) 27005
doi: 10.1209/0295-5075/99/27005

www.epljournal.org

Strain-induced phase transition in β-MnO_2

Xing Huang[1,2], X. H. Yan[1,3(a)], Y. Xiao[1], Y. D. Guo[1], Z. H. Zhu[4] and C. J. Dai[1]

[1] *College of Science, Nanjing University of Aeronautics and Astronautics - Nanjing, 210016, China*
[2] *School of Mathematics and Physics, Nanjing University of Information Science and Technology Nanjing, 210044, China*
[3] *School of Electronic Science and Engineering, Nanjing University of Posts and Telecommunications Nanjing, 210046, China*
[4] *Department of Physics, University of Connecticut - Storrs, CT 06269, USA*

received 21 June 2012; accepted in final form 28 June 2012
published online 30 July 2012

PACS 75.25.-j – Spin arrangements in magnetically ordered materials (including neutron and spin-polarized electron studies, synchrotron-source X-ray scattering, etc.)
PACS 71.30.+h – Metal-insulator transitions and other electronic transitions
PACS 85.75.-d – Magnetoelectronics; spintronics: devices exploiting spin polarized transport or integrated magnetic fields

Abstract – The phase transition of β-MnO_2 under negative pressure and external strain was investigated via the density function theory. During the expansion, the half-metallic phase appeared. Using the Heisenberg model, the variations in the exchange integrals between Mn^{4+} pairs were determined. A crossover between the dominate exchange integrals occurred, which resulted in the formation of the ferromagnetic phase. On the other hand, the double exchange mechanism and weakening of the crystal field were the two reasons for the formation of the majority of conduction bands.

Introduction. – β-MnO_2, which crystallizes in the same manner as the half-metallic (HM) material CrO_2 [1], is known for its complex magnetic structure below T_N ($\sim 92\,\mathrm{K}$) [2]. Neutron diffraction revealed that the magnetic unit cell of MnO_2 is seven times larger than the chemical unit cell along the c-axis [3]. The following theoretical studies proposed that the local magnetic moments in MnO_2 are helically arranged [3,4]. This helical magnetic order, together with the strong Coulomb correlation between Mn $3d$, confers various electromagnetic properties to MnO_2, which has gained increasing attention both theoretically and experimentally among researchers [5–8]. Thus far, MnO_2 has been epitaxially grown on a TiO_2 substrate by molecular beam epitaxy [5]. For the lattice mismatching, MnO_2 is strained. Studies have shown that the epitaxial strain modifies the magnetic easy axis of the CrO_2 film because lattice mismatching produces magnetoelastic anisotropy energy [6–9]. Moreover, the lattice expansion can determine the relative strength of two instabilities in the $BaMnO_3$ bulk by inducing the second order John-Teller off-center distortion in the non-d^0 magnetic cations [10]. However, little is known about the strain-dependent effect in MnO_2. In this work, MnO_2 under external strain was studied. We investigated the influence of volume expansion on the property of the MnO_2 bulk and the expansion strain loaded on the (a,b)-plane or c-axis to understand the behavior of MnO_2 under tensile strain.

Calculation details. – The property of the MnO_2 bulk was determined by the density functional theory (DFT) [11] using the VASP code [12,13]. A unit cell with a P42/mnm symmetry containing two Mn atoms and four O atoms was built (except for calculating the exchange parameter J_2 or J_3, $1\times1\times2$ or $2\times1\times1$ supercells were used according to the magnetic structure, which will be discussed in detail in the last three paragraphs). The generalized gradient approximation (GGA) [14] was performed to determine the exchange-correlation effects, whereas the projector augmented wave [15] potential is used to describe the interaction between atoms and electrons. A $5\times5\times9$ k-grid was sampled via the Monkhost-Pack scheme in the Brillouin zone, and a plane wave energy cutoff of 520 eV was chosen to fully converge the total energy. For the on-site Coulomb correlations in the Mn $3d$ orbitals, the Hubbard parameter U and exchange parameter J were taken into account using the fully localized

(a) E-mail: xhyan@nuaa.edu.cn

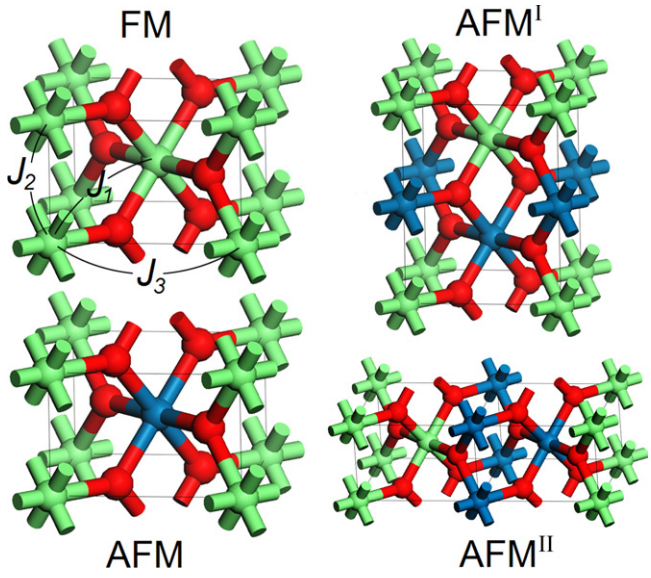

Fig. 1: (Color online) Structures of the MnO_2 bulk. FM, AFM, AFM^{I}, and AFM^{II} are the different magnetic structures considered in our calculations. Red spheres indicate oxygen atoms, whereas green and blue balls indicate spin-up and spin-down Mn atoms, respectively. The paths of exchange interactions are also shown.

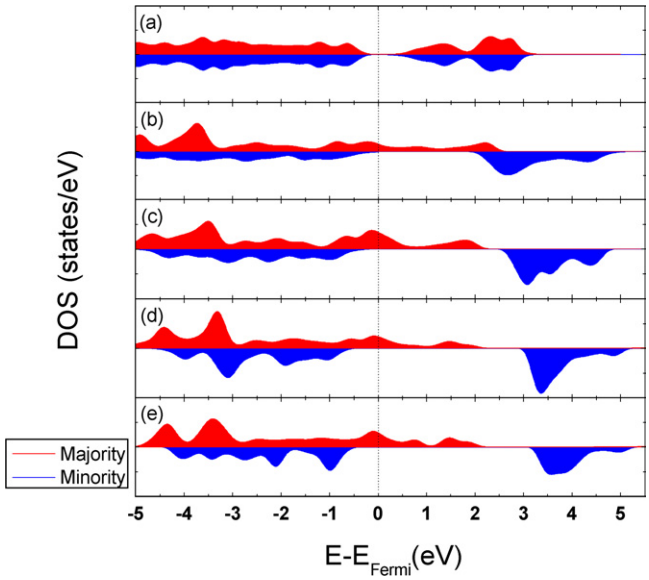

Fig. 2: (Color online) DOS of the MnO_2 bulks with different expansion rates. (a) DOS of the unstrained bulk; (b)–(e) the volume increased by 5%, 10%, 15%, and 20%, respectively.

limit (FFL) GGA+U method [16,17]. The values of U and J were set at 4 eV and 0.9 eV according to previous studies, respectively [18–20]. During relaxation, all atoms are allowed to move until the Hellmann-Feynman forces acting on them become less than 0.01 eV/Å.

Our results are mainly based on a collinear magnetic arrangement, which is similar to the study by Franchini *et al.* on manganese oxides [18]. The antiferromagnetic (AFM) and ferromagnetic (FM) phases (as shown in fig. 1) were compared, and only the most stable phase is discussed. We also consider the non-collinear magnetic structure in the last part of our discussion to make our results more reliable.

Results and discussion. – After structure optimization, the lattice constants a and c are 4.46 and 2.91 Å, respectively. These values agree with the experimental findings ($a = 4.40$ Å, $c = 2.87$ Å). Figure 2(a) shows the density of states (DOS) of the unstrained bulk. The symmetrical DOS for the majority and minority spins reveals the AFM phase. The local magnetic moment of each Mn atom is $2.9\mu_B$, which corresponds to the +4 oxidation state of the element. As shown in fig. 2(a), a gap across the Fermi level (E_F) is observed, which can be traced to the splitting of Mn 3d. This splitting is driven by the O octahedron around Mn. According to the crystal field (CF) theory, the O CF would split the Mn 3d into a low-lying t_{2g} triplet and a higher e_g doublet. The t_{2g} triplet shifts down below E_F, which corresponds to the three remaining 3d electrons of Mn^{4+}, whereas the e_g doublet shifts above E_F. Thus, the gap is formed.

Volume expansion was also performed. The lattice expands to all directions by the same ratio, which is similar to previous findings [10,21,22]. The volume expansion can be considered a negative hydrostatic pressure. In practice, this condition is difficult to achieve, but the theoretical studies on the effect of negative pressures can help us understand the phenomenon in the strained MnO_2 films better [23]. Figure 2(b) shows the DOS when the cell volume is expanded to 105%. The majority states are spread across the E_F, whereas a gap larger than 1 eV splits the minority states. The total magnetic moment of the unit cell is $6.0\mu_B$. The spin-down gap, together with the integral magnetic moment, strongly indicates that the HM phase exists. A value of $6.0\mu_B$ per unit cell also implies that the FM magnetic moment arrangement between Mn^{4+} retains its three 3d electrons after stretching. When the volume further expands, the HM property is maintained, as shown in figs. 2(c)–(e). Moreover, the spin-down gap increases with volume expansion. The main conduction and magnetic properties of the strained bulk are listed in table 1. The strained bulk generally stabilizes in the HM phase if the volume is expanded beyond 105%. We also consider different U ranging from 0.9 eV to 5 eV, and similar results are obtained.

The origin of the conduction bands across E_F must be determined to understand the formation of the HM phase better. In fig. 3(a), we draw the local density of states (LDOS) for Mn 3d and O 2p when the cell volume was expanded by 110%. For the majority spin, the main part of e_g is above E_F, whereas t_{2g} is just below E_F. Unlike in the unstrained bulk, t_{2g} and e_g overlap each other. Thus, the DOS across E_F becomes non-zero. Meanwhile, the minority 3d states are fully

Table 1: Conduction and magnetic properties of the strained MnO_2 bulks with different expansion ratios. M is the total magnetic moment per unit cell, and * is the half-metallic (HM) phase. J_1, J_2, and J_3 are the exchange integrals obtained from our calculation using the Heisenberg model.

	a, b, c fixed		a, b fixed				c fixed			
Expansion ratio	M (μ_B)	J_1 (meV)	M (μ_B)	J_1 (meV)	J_2 (meV)	J_3 (meV)	M (μ_B)	J_1 (meV)	J_2 (meV)	J_3 (meV)
100%	0	−2.06	0	−2.06	−2.87	−2.06	0	−2.06	−2.87	−2.06
105%	6.00*	2.75	0	−0.09	−1.69	−0.31	0	−1.97	−3.06	−1.75
110%	6.00*	10.69	6.00*	3.72	5.06	5.56	6.00*	0.59	1.75	1.13
115%	6.00*	14.06	6.00*	8.77	31.28	5.03	6.00*	4.20	12.66	7.84
120%	6.00*	9.66	6.00*	4.55	76.59	0.30	6.00*	7.81	30.94	10.44

pushed up above E_F from the O $2p$ states because of the strong d-d exchange interaction, which leads to the spin-down gap. The distribution of the Mn $3d$ minority states becomes more local after being stretched (as shown in fig. 2). The overlap of the t_{2g}-e_g majority states are partly attributed to the weakening of the O CF. When the lattice expands, the O octahedron also expands. The interaction between the Mn $3d$ and the O octahedrons are also weakened, which reduces the t_{2g}-e_g splitting. This relatively smaller splitting is the first reason for the formation of the conduction bands, shown as reason I in fig. 3(c).

Another reason for the formation of the conduction band is the involvement of O $2p$ during t_{2g}-e_g overlapping. As shown in fig. 3(a), the O $2p$ states hybridize with the Mn e_g states near E_F, which implies strong p-d hybridization. This hybridization can also be found in the HM phase of the $BaMnO_3$ bulk [22]. The majority-spin band structure is given in fig. 3(b) to provide more details of the hybridization. The four bands above E_F are mainly produced by the e_g states. In some areas, these bands are quite flat, which indicates the pure $3d$ feature. Meanwhile, in other areas, these bands are dispersed. In such areas, the contributions of the O $2p$ states in the bands are greater. Some parts of these bands spread across E_F and overlap with the t_{2g} bands. This phenomenon produces the majority conduction channel. This phenomenon strongly indicates that a double exchange occurs. When the local spin positions are parallel to each other, the double exchange mechanism improves the localized e_g electron transfer from one Mn ion to another, which causes a decrease in energy. This behavior may the key reason for the overlap of t_{2g}-e_g. Through the participation of O $2p$, Mn e_g bands become more dispersed. For the decrease in the energy difference due to reason I, the strong dispersion finally leads to the overlap between the adjacent e_g and t_{2g} bands. This process is shown as reason II in fig. 3(c). These two reasons function synchronously, but the effect of reason II is more significant. The O $2p$-mediated strong band dispersion can explain why the Coulomb reputation cannot open the majority gap between t_{2g} and e_g. Similar findings are also observed in the CrO_2 bulk [1].

However, as discussed by Sato *et al.*, the double exchange cannot determine the magnetic structure in the unstrained MnO_2 bulk [2]. Other exchange interactions, such as superexchange, exist. Therefore, the effective exchange integrals between Mn^{4+} ions can be considered as the total effect of all these exchange interactions. The variations in the exchange integrals need to be determined to interpret the AFM-FM transition. Thus far, the Heisenberg model has been used to determine various kinds of magnetic coupling in transition metal complexes [3,24–28]. In the present study, we use the classical Heisenberg model to estimate the exchange integral between the Mn pairs. In the classical Heisenberg model, the quantum fluctuation is negligible, and the local spins are treated as classical vectors. In MnO_2, the exchange coupling energy induced by the Mn pairs can be expressed as $H_{ij} = -J_n \mu_i \cdot \mu_j$, where μ_i and μ_j are the local magnetic moments of the neighboring Mn_i and Mn_j, respectively, whereas J_n stands for the exchange integral between the Mn_i and Mn_j. We can substitute $|\mu_i|$ and $|\mu_j|$ into J and treat the local spins as unit vectors because $|\mu_i| = |\mu_j| = 3\mu_B$ remains unchanged during the expansion [24]. Three exchange integrals mainly exist in the MnO_2 bulk [3] As shown in fig. 1, J_1 is between the neighboring Mn^{4+} pairs along (111), whereas J_2 is along (001), and J_3 is along (100). Thus, the total energy per unit cell can be expressed as

$$E = E_0 - \sum_{ij} J_n \cos\theta_{ij},$$

where θ_{ij} is the angle between the localized spins μ_i and μ_j, and i and j are dependent on n ($n = 1, 2$ *or* 3) in J_n. E_0 is the energy independent of the magnetic structure.

For the FM phase, $\theta_{ij} = 0$. Therefore, the total energy per unit cell is expressed as

$$E_{FM} = E_0 - 16J_1 - 4J_2 - 8J_3.$$

Correspondingly, for the AFM phase (marked as MnF_2-type antiferromagnetic structure in Yoshimori's work [3]), the total energy can be expressed as

$$E_{AFM} = E_0 + 16J_1 - 4J_2 - 8J_3.$$

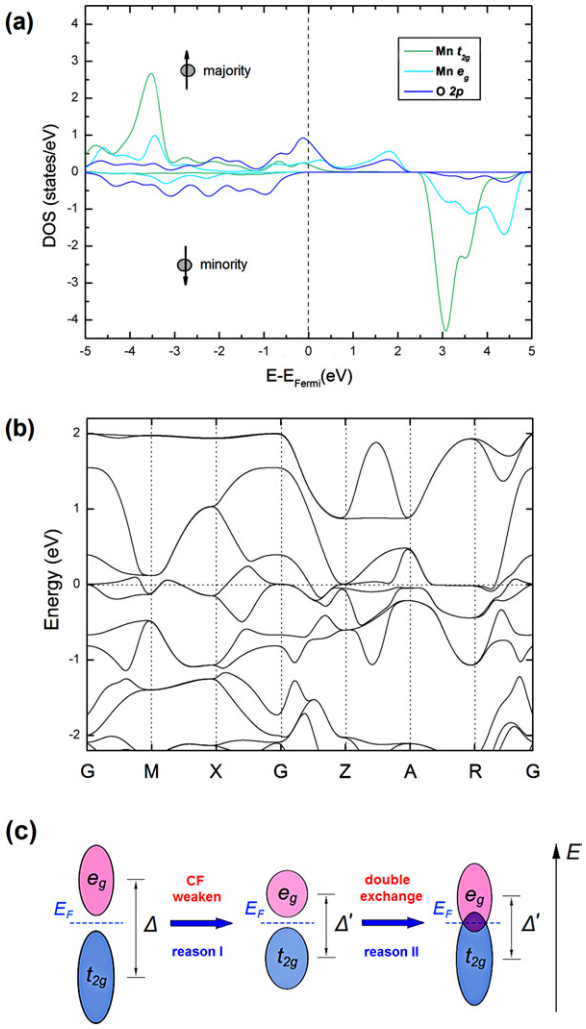

Fig. 3: (Color online) (a) LDOS of Mn $3d$ and O $2p$ for the MnO_2 bulk when the cell volume was expanded to 110%. Green curves stand for Mn t_{2g} states, whereas cyan curves stand for e_g states. Blue curves represent O $2p$ states. (b) Band structure of the strained bulk, for majority spin. (c) The two reasons for the t_{2g}-e_g majority overlap, marked by reason I and reason II. e_g and t_{2g} are the majority-spin states of Mn $3d$. Δ and Δ' are the splitting energies between the t_{2g} and e_g centers. Δ represents the case in the unstrained bulk where CF is much stronger, whereas Δ' is the splitting energy in the weakened CF. According to the CF theory, $\Delta > \Delta'$.

Comparing the two equations above, we can find that J_1 determines the competition between the FM and AFM phases. We can obtain J_1 using

$$J_1 = (E_{AFM} - E_{FM})/32.$$

Using the equation above, E_{FM} and E_{AFM} can be obtained. The calculated J_1 for different cell volumes are listed in table 1. J_1 is positive in the unstrained bulk, which implies that the AFM phase is more stable than the FM phase. However, when the cell volume size expands by 5%, J_1 becomes negative, which indicates that the bulk shifts to the FM phase. When the cell volume

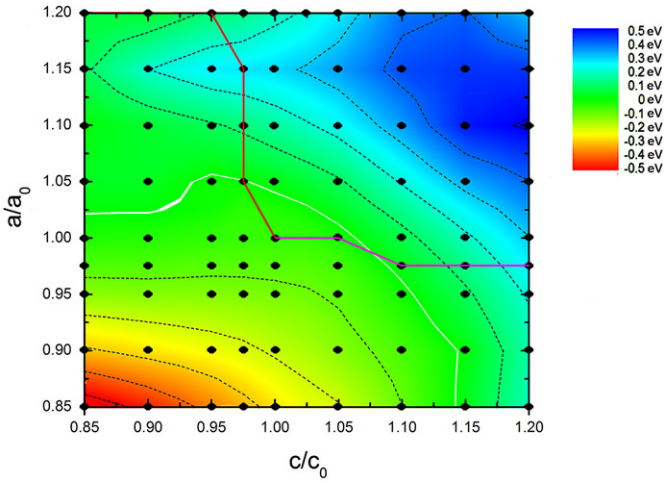

Fig. 4: (Color online) (a) Red curve represents changes in c when a and b are fixed, whereas the pink curve shows the changes in a and b when c is fixed. a_0 and c_0 are the lattice parameters of the unstrained bulk. The background shows the energy difference between the FM and AFM phase ($E_{AFM} - E_{FM}$). The black dots are the sampling points considered in our calculation.

further expands, J_1 becomes more negative (except for an expansion of 120%, where J_1 nearly becomes zero due to the excessively long distance between two Mn^{4+}). This trend is consistent with Néel and Slater's deduction, which states that when the distance between the cations becomes larger, the localized spins become arranged in an FM order [29,30]. Thus, we can conclude that the lattice expansion causes the exchange integral J_1 to become negative, which transfers the bulk to the FM phase. As soon as the FM phase is formed, the double exchange closes the majority gap. Thus, the bulk HM property is formed.

We also consider a more realistic case, in which the lattice is stretched along one or two directions. This phenomenon can be achieved by applying epitaxial strain to the lattice. We first fixed the lattice constant a, b with a given expansion ratio, which correspond to an in-plane tensile stress. The proper length of c was then obtained to make the strained bulk reach the minimal total energy. We then drew the DOS for each case to determine if the AFM-FM transition happens. As shown in fig. 4, the red curve displays the changes in c when a and b are stretched. c decreases from 100% to 95% during the expansion process. The energy differences ($E_{AFM} - E_{FM}$) when a, b, and c are all sampled are shown in fig. 4. The lower left area is the AFM-dominant area, whereas the top right area is the FM-dominant area. The white belt represents the FM-AFM boundary. The red curve intersects the white belt when a and b are expanded by 6%, which imply that an AFM-FM transition occurs. We then examine the conduction property of these FM phases. The HM property appears when the FM phase appears, which is similar to the aforementioned results. We also

consider the case when only c is extended, as shown by the pink curve in fig. 4. The FM phase appears when the length of c is expanded beyond 8%. This relative larger expansion ratio needed for the AFM-FM phase transition may be attributed to the smaller original length of lattice parameter c compared with those of a and b. The FM phase also exhibits the HM property, as shown in table 1. In summary, when properly expanded along the a and b (>106%) or c (>108%) axes, the strained bulk favors the HM phase, which is similar to the all-direction expansion.

As mentioned before, all results above were obtained by considering only the collinear magnetic structure. However, as pointed out by Yoshimori, the screw-type spin arrangement is more stable in the unstained bulk compared with the AFM phase [3]. Hence, the helical spin states and other magnetic structures need to be considered to examine the stability of the HM phase. The magnetic structure is dependent on the values of J_1, J_2, and J_3. For example, if $J_1 < 0$ and J_2 and $J_3 > 0$, the MnF_2-type magnetic structure would be dominant. Similarly, when the helical magnetic structure appears, J_2 or $J_1 > 1$ and J_1 and $J_2 < 0$ must be fulfilled. We already obtained the value of J_1, but J_2 and J_3 are remain unknown. Thus, we consider two other kinds of magnetic structures (marked by AFM^{I} and AFM^{II} in fig. 1) to obtain J_2 and J_3. These two magnetic phases are more complex than the FM or AFM phase mentioned before. Therefore, the supercell containing two super cells was used in the calculation. The total energy per unit cell for the two magnetic structures can be expressed as

$$\begin{aligned} E_{AFM^I} &= E_0 + 4J_2 - 8J_3, \\ E_{AFM^{II}} &= E_0 - 4J_2. \end{aligned}$$

With the two additional equations above, J_2 and J_3 can be obtained as follows:

$$\begin{aligned} J_2 &= (2E_{AFM^I} - E_{FM} - E_{AFM})/16, \\ J_3 &= (2E_{AFM^{II}} - E_{FM} - E_{AFM})/16. \end{aligned}$$

Table 1 lists the values of J_1, J_2, and J_3 when a, b, or c is expanded and fixed. In the unstrained bulk, J_1, J_2, and J_3 are negative. When $J_2 > J_1$ the helical magnetic structure can exist. However, as the cell volume increases, a crossover corresponding to the AFM-FM transition between J_1 occurs (see table 1). Meanwhile, J_2 and J_3 also become positive. When J_1, J_2, and $J_3 > 0$, the helical magnetic structure, as well as the other AFM phases, become unstable. As a result, the HM phase remains in the strained bulk.

Conclusion. – In summary, using the DFT + U scheme, the magnetic and conduction properties of MnO_2 under negative pressure and tensile strain are investigated. Under specific strain values, the FM phase is more dominant than AFM. The formation of the FM phase may be driven by the lattice expansion, which converts the exchange integrals J_1, J_2, and J_3 into positive values. As soon as the FM phase appears, the HM property can be obtained synchronously, which is induced both by the weakening of O CF and by the O 2p-mediated double exchange between Mn 3d orbitals. Our results may provide a reference for the epitaxial growth of HM MnO_2 on specific substrates for spintronic applications.

* * *

This work was supported by the National Natural Science Foundation of China (NSFC10874089 and NSFC51032002), the key project of National High Technology Research and Development Program of China (2011AA050526), the Science and Technology Support Plan of Jiangsu Province (BE2011191), and the Funding of Jiangsu Innovation Program for Graduate Education (CXZZ11_0190 and CX08B_005Z).

REFERENCES

[1] Korotin M. A., Anisimov V. I., Khomskii D. I. and Sawatzky G. A., *Phys. Rev. Lett.*, **80** (1998) 4305.
[2] Sato H., Enoki T., Isobe M. and Ueda Y., *Phys. Rev. B*, **61** (2000) 3563.
[3] Yoshimori A., *J. Phys. Soc. Jpn.*, **14** (1959) 807.
[4] Osmond W. P., *Proc. Phys. Soc.*, **87** (1966) 335.
[5] Chambers S., *Surf. Sci.*, **420** (1999) 123.
[6] Spinu L., Srikanth H., Gupta A., Li X. W. and Xiao G., *Phys. Rev. B*, **62** (2000) 8931.
[7] Rameev B. Z., Gupta A., Miao G. X., Xiao G., Yildiz F., Tagirov L. R. and Aktas B., *Phys. Status Solidi A*, **201** (2004) 3350.
[8] Miao G. X., Xiao G. and Gupta A., *Phys. Rev. B*, **71** (2005) 094418.
[9] Pathak M., Sato H., Zhang X., Chetry K. B., Mazumdar D., LeClair P. and Gupta A., *J. Appl. Phys.*, **108** (2010) 053713.
[10] Rondinelli J., Eidelson A. and Spaldin N., *Phys. Rev. B*, **79** (2009) 205119.
[11] Kohn W. and Sham L. J., *Phys. Rev.*, **140** (1965) A1133.
[12] Kresse G. and Furthmüller J., *Phys. Rev. B*, **54** (1996) 11169.
[13] Kresse G. and Furthmüller J., *Comput. Mater. Sci.*, **6** (1996) 15.
[14] Wang Y. and Perdew J. P., *Phys. Rev. B*, **43** (1991) 8911.
[15] Blöchl P. E., *Phys. Rev. B*, **50** (1994) 17953.
[16] Liechtenstein A. I., Anisimov V. I. and Zaanen J., *Phys. Rev. B*, **52** (1995) R5467.
[17] Dudarev S. L., Botton G. A., Savrasov S. Y., Humphreys C. J. and Sutton A. P., *Phys. Rev. B*, **57** (1998) 1505.
[18] Franchini C., Podloucky R., Paier J., Marsman M. and Kresse G., *Phys. Rev. B*, **75** (2007) 195128.
[19] Anisimov V., Zaanen J. and Andersen O. K., *Phys. Rev. B*, **44** (1991) 943.
[20] Satpathy S., Popovic Z. and Vukajlovic F., *Phys. Rev. Lett.*, **76** (1996) 960.
[21] Zhu Z. H. and Yan X. H., *J. Appl. Phys.*, **106** (2009) 023713.

[22] Li N., Yao K. L., Sun Z. Y., Zhu L. and Gao G. Y., *J. Appl. Phys.*, **109** (2011) 083715.
[23] Yong L., Lihong N., Zhaohui R., Gang X., Chenlu S. and Gaorong H., *J. Phys.: Condens. Matter*, **21** (2009) 275901.
[24] Sims H., Oset S. J., Butler W. H., MacLaren J. M. and Marsman M., *Phys. Rev. B*, **81** (224436).
[25] da Silva A. J. R., Fazzio A., dos Santos R. R. and Oliveira L. E., *Phys. Rev. B*, **72** (2005) 125208.
[26] Jiang X. F. and Guo G. Y., *Phys. Rev. B*, **70** (2004) 035110.
[27] Lv S., Li H., Liu X., Han D., Wu Z. and Meng J., *J. Phys. Chem. C*, **114** (2010) 16710.
[28] Perring T. G. Aeppli G. Hayden S. M. Carter S. A. Remeika J. P. Cheong S. W., *Phys. Rev. Lett.*, **77** (1996) 711.
[29] Néel L., *Ann. Phys. (Paris)*, **8** (1937) 227.
[30] Slater J. C., *Phys. Rev.*, **36** (1930) 57.